Measurement of gravitation-induced quantum interference for neutrons in a spin-echo spectrometer

Victor-O. de Haan
BonPhysics BV, Laan van Heemstede 38, 3297AJ Puttershoek, The Netherlands

Jeroen Plomp, Ad A. van Well, and M. Theo Rekveldt
Department Radiation Science and Technology, Faculty of Applied Sciences, Delft University of Technology, Mekelweg 15, 2629 JB Delft, The Netherlands

Yuji H. Hasegawa
Atominsitut, Vienna University of Technology, A-1020 Vienna, Austria

Robert M. Dalgliesh and Nina-Juliane Steinke
STFC, ISIS, Rutherford Appleton Laboratory, Chilton, Oxfordshire, OX11 0QX, United Kingdom
(Received 31 March 2014; published 12 June 2014)

With a neutron spin-echo reflectometer (OffSpec at ISIS, UK) it is possible to measure the gravitation-induced quantum phase difference between the two spin states of the neutron wave function in a magnetic field. In the small-angle approximation, this phase depends linearly on the inclination angle of the neutron beam with respect to the horizontal. This also holds for the Bonse-Hart interferometer used in the Colella-Overhauser-Werner experiments and should be taken into account. Neglecting this term could yield deviations up to 1% per degree inclination angle. The gravitation-induced quantum phase as measured with OffSpec with an accuracy of 0.1% agrees with the theoretically expected results.

DOI: 10.1103/PhysRevA.89.063611 PACS number(s): 03.75.Be, 14.20.Dh, 04.80.Cc

I. INTRODUCTION

Gravity is one of the most profound physical forces we encounter in daily life. Although we can measure gravity in classical mechanics with high precision, we do not know the exact origin of this force. To come to a deeper understanding, we need to understand the way gravity acts on a quantum system. One of the quantum systems on which gravity acts is the free neutron.

A neutron can be viewed classically as a particle with mass or quantum mechanically as a wave, as envisaged by De Broglie. Similar to all matter waves, neutrons are endowed with a magnetic moment that allows for Larmor precession in a magnetic field. An advantage of neutrons is that they are charge and electric-dipole-moment free, hence free from strong electronic interactions. The quantum-mechanical equivalent description is by means of two coupled wave functions (spin-up and spin-down eigenfunctions) that can be distinguished in a magnetic field.

Classically, the neutron will just fall as a particle with mass in a gravitational field like any other particle. This has been experimentally detected in 1965 by Dabbs [1] and repeated with increased accuracy by Koester [2] and Schiedmayer [3]. The results show a correspondence up to a measurement accuracy of 0.02%.

In the wave picture, one can split the wave function into wave packets and let them travel through different potentials (heights) in this gravitational field. Already in 1975 Colella *et al.* [4] showed, using a Bonse-Hart interferometer for neutrons, that a quantum-mechanical phase of the neutron is induced by the average height difference of these wave functions (COW experiments). Later these COW experiments were repeated with greater precision, including all possible corrections, and an approximate -1% $(+/-0.1\%)$ discrepancy was found with theory. All COW experiments reported a phase shift that was too small with respect to the expected gravitational effect [5]. Littrell discusses the influence of dynamical refraction in the interferometer [6]. Although the influences are of similar order as the observed differences, he was not able to fully explain the experimental results. Further efforts are underway to repeat the COW experiment with an adapted interferometer, greatly reducing the influence of these systematic effects [7]. It is very difficult, however, to avoid distortions (and the resulting phase shift) of an interferometer made of a perfect silicon crystal.

Recently, gravity measurements with neutrons and atoms aroused new interest on account of the gravitational redshift, Compton frequency, time dilation, etc. (see Ref. [8] and references therein).

In view of the above, an experiment on the influence of gravity on the quantum-mechanical phase of the neutron wave has been devised, built, and executed. Precise measurement of this kind enables a measurement of the Lorentz invariance violation induced by the gravitational forces [9] in the future.

II. METHOD

The spin-echo mode of the polarized-neutron spectrometer OffSpec [10,11] is, in fact, a quantum-interferometer-based technique [12]. Initially the polarization of the neutron beam is parallel to the magnetic field. Spin-up and spin-down eigenstates are created by means of a step in a magnetic field. The field directions before and after the step are perpendicular. Before the step the polarization vector is parallel to the magnetic field, and after the step is it perpendicular to the polarization vector. In this way the amplitudes of the two spin-eigenstates directly after the step are the same, although their initial phase differs by $\pi/2$ radians. After that, in the first

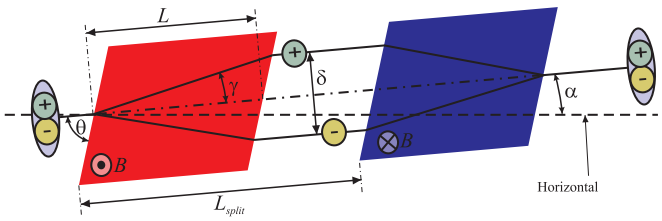

FIG. 1. (Color online) Scheme of the polarized neutron interferometer OffSpec. In the first half of the instrument one separates the spin-up and spin-down eigenstates in space by a magnetic field, just to bring them back together in the second half of the instrument by a mirrored field configuration. After that, the spin states interfere constructively (when in phase) or deconstructively (when out of phase). If the splitting is in the horizontal plane, the spin states will acquire the same phases and the spin-up and spin-down eigenstates remain in phase. If the splitting is in the vertical plane, the spin states will acquire different phases due to the differences in gravitational potential in one arm with respect to the other arm and the interference changes accordingly.

half of the instrument one separates the spin-up and spin-down eigenstates in space by a magnetic field just to bring them back together in the second half of the instrument by a mirrored field configuration (see Fig. 1). After the neutrons leave the second magnetic-field region there is again a magnetic-field step. When the phase difference between the eigenstates is again $\pi/2$ radians, the spin eigenstates interfere constructively and the polarization is again parallel to the magnetic field or when out of phase, the spin eigenstates interfere destructively, reducing the polarization. The intensity due the polarization component parallel to the magnetic field is detected after another polarizer.

When a sample is present between the two magnetic fields and scattering occurs, the eigenstates travel a different path through the second half of the instrument, resulting in a phase difference and therefore a change in interference pattern. In the case of the absence of a sample, one will retrieve the original interference (i.e., the spin-echo signal as a function of wavelength).

If the splitting is in the horizontal plane, the spin states will acquire the same phases and the spin-up and spin-down eigenstates remain in phase. If the splitting is in the vertical plane, the spin states will acquire different phases due to the differences in gravitational potential in one arm with respect to the other arm and the interference changes accordingly. The up-down eigenstate interference is measured by the detector behind the analyzer (not shown), where the intensity recorded is

$$I^{\pm} = I_s \frac{1 \pm P \cos \Delta\phi}{2}, \tag{1}$$

where I_s equals the so-called shim intensity, P is the polarization of the beam, $\Delta\phi$ is the phase difference of the two spin states as acquired on their different paths through the instrument, and $\pm$ denotes the detection of the spin-up $(+)$ or spin-down $(-)$ eigenstate.

Solving the Schrödinger equation for a quantization axis parallel to the magnetic induction yields plane waves with a wave vector given by $k^{\pm} = n^{\pm} k_0$. $k_0 = 2\pi/\lambda$ is the wave vector of the neutron in vacuum, where λ equals the wavelength of the neutron. The refractive index $n^{\pm}$ for each spin state can be calculated according to

$$n^{\pm} = \sqrt{n_0^2 \mp \epsilon_z}, \tag{2}$$

where $\epsilon_z = 2m\mu_n B/(\hbar^2 k_0^2)$ is the ratio between the Zeeman energy and the kinetic energy of the neutron, where m is the neutron mass, $\hbar$ Planck's constant divided by 2π, μ_n the neutron magnetic moment, and B the magnetic flux density. $n_0 = \sqrt{1 - 2mV/(\hbar^2 k_0^2)}$ equals the refractive index when the magnetic field is absent, where V is the optical potential [13]. The optical potential is determined by a term due to the material the neutrons are traveling through and a term due to gravity,

$$V = \frac{2\pi\hbar^2}{m}\langle Nb\rangle + V_g,$$

where $\langle Nb\rangle$ is the average scattering-length density of the material and V_g is the gravitational potential of the neutron. Here, the neutron travels through air and the average scattering-length density is taken 0. If a neutron beam crosses a boundary of a magnetic flux density region and the border is not perpendicular to the propagation direction, so-called beam splitting occurs due to birefringence, as shown in Fig. 1. At the boundary the parallel component of the wave vector is continuous, which gives Snell's law,

$$k \cos\theta = k^{\pm} \cos(\theta - \gamma^{\pm}),$$

where k is the wave vector in zero magnetic field and $k^{\pm}$ the wave vector of the spin-up $(+)$ or spin-down $(-)$ wave function, and θ is the angle between the wave vector and the front face of the magnetic-field region. Note that k is the value of the wave vector for the optical potential at the location where refraction occurs. Under the condition that $\epsilon_z \ll 1$, the refraction angle is

$$\gamma^{\pm} = \pm \frac{\epsilon_z}{2n_0^2} \cot\theta. \tag{3}$$

For a magnetic flux density of 1/3 T, $\theta = 45^{\circ}$, and for a neutron wavelength λ of 0.2 nm, $\gamma = |\gamma^{\pm}| \approx 0.5$ μrad. The spin-down wave is refracted at the boundary with an angle exactly opposite to the one of the spin-up wave. This directly explains the beam splitting, and the splitting distance or spin-echo length is

$$\delta = 2L\gamma = \frac{2m\mu_n BL \cot\theta}{\hbar^2 k_0^2 n_0^2} = \eta\lambda^2. \tag{4}$$

Note that this spin-echo length is proportional to the square of the wavelength, where the proportionality constant η is the spin-echo-length constant determined by neutron properties and instrument settings only. As pointed out above, not only can a sample change the phases, but so can a difference in gravitational potential. If the splitting of the eigenstates is in the horizontal plane, they will travel through the same potential and no gravitation-induced phase difference occurs. If the splitting is in the vertical plane, a gravitation-induced phase does occur and the interference pattern changes. In Appendix A the phase difference is derived assuming that the curvature of

the trajectories can be neglected. The result is

$$\Delta\phi_g = \frac{Am^2g}{\hbar^2 k_0}(1 - \alpha \tan\theta),$$

where $A = L_{\text{split}}\delta$ is the area between the path of the two spin states and α is the inclination angle between the wave vector of the neutron entering the interferometer and the horizontal. For $\alpha = 0$ this corresponds to the phase difference obtained in literature for the COW experiments [4,14]. In literature it is assumed that the incident beam is exactly in the horizontal plane and the interferometer rotates around this beam. It is assumed that if the beam has a small inclination angle with the horizontal, then the phase difference is changed only by second order in the inclination angle. The argument used is that the projection of the gravitation on the vertical is proportional to the cosine of this inclination angle. In Appendix A we show that this is not correct for the current experiment and that the correction term is linear in the inclination angle. Interestingly, the same holds for the COW experiment itself when in the above formula θ is replaced by the Bragg angle θ_B, as derived in Appendix A.

III. CALIBRATION

To obtain accurate results for the gravitation-induced phase difference, several instrumental parameters need to be calibrated. The instrument parameters influencing the results are the measurement of the neutron wavelength λ, the inclination angle with the horizontal α, the distance between the magnetic-field regions L_{split}, and the spin-echo-length constant η.

The neutron wavelength is measured by the time-of-flight method, where the flight time of the neutron over a known distance is determined. From this flight time and distance the velocity of the neutron can be calculated and hence its wavelength. For OffSpec the wavelength scale has been checked with transmission measurements of aluminum. The transmission was fitted using the method described in [15]. The relevant lattice parameter of the aluminum sample was calibrated against a NIST Si reference powder SRM640c at the High Resolution Powder Diffractometer at ISIS [16], resulting in 0.404 919(1) nm. The resulting accuracy of the instrumental wavelength is 5×10^{-4} nm, which is 0.05% at 1-nm wavelength.

The inclination angle of the instrument is fully automated and was checked by comparing the reflection angle on a liquid surface with the one set according to the instrument. The accuracy is 0.1 mrad. The distance L_{split} between the magnetic-field regions was measured with calibrated measuring rods up to 0.1 mm accuracy and was 3850.0 mm.

The spin-echo-length constant was calibrated by measuring the small-angle structure factor of a calibration sample. The measured polarization [Eq. (5)] depends both on the phase difference and the polarization of the beam. The polarization of the beam is reduced when a sample with a structure on the same length scale as the spin-echo length is inserted. This is the basis of the Spin-Echo Small Angle Neutron Scattering technique [17]. The polarization change can be accurately calculated using the phase-object approximation [18]. The calibration sample was a silicon grating with a period of 6.000 μm. It was constructed by means of interferometric lithography with visible light with a relative accuracy of a fraction of a wavelength over a distance of a at least 1 cm, and hence with an estimated accuracy of 0.01%.

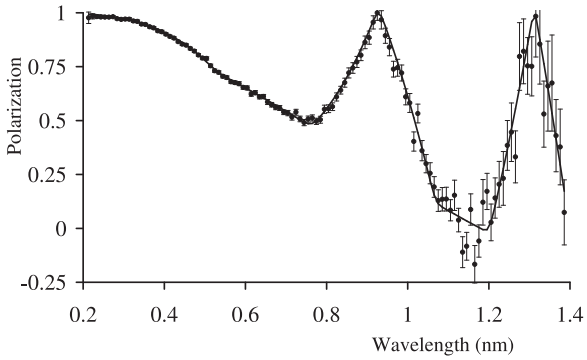

FIG. 2. Ratio of beam polarization with grating in the beam to empty beam polarization as a function of wavelength for the instrument setting $\alpha = -1^{\circ}$. The line is a fit using the phase-object approximation.

When the period of the grating is equal to the spin-echo length, a maximum in the interference occurs. Hence, by measuring the beam polarization change due to the grating, the spin-echo-length constant can be determined *in situ* under exactly the same instrumental conditions as for the gravitational phase difference measurements. This has been done for all the instrumental settings used in the experiment. An example is shown in Fig. 2 for a measurement with $\alpha = -1^{\circ}$ and $\theta = 50^{\circ}$. The data points, including error bars, represent the ratio between the beam polarization, including the sample, and the empty beam polarization. The line represents this ratio calculated for a trapezium-shaped grating profile with a repetition period of 6.000 μm, a top width of 1709 μm, and a base width of 3791 μm. The height of the trapezium was 8.931 μm. For these settings the fitted spin-echo-length constant $\eta = 7.002(18)\ \mu\text{m/nm}^2$. As the grating was the same for all measurements, the height, top width, and base width of the grating were fitted to all measurements together. Furthermore, the measurements showed no influence of the inclination angle of the instrument with the horizontal, α on the spin-echo-length constant. This is to be expected because the complete setup (including magnets and beam diaphragms) was rotated around one point to change the inclination angle. The effective angle θ for the instrumental settings used can be calculated according to Eq. (4), yielding 55.30(7)$^{\circ}$.

IV. MEASUREMENTS AND RESULTS

The measurements consist of determining the polarization of the beam by measuring the spin-up and spin-down eigenstate intensity at the detector [19] as a function of the spin-echo phase difference according to Eq. (1):

$$P_m = \frac{I^+ - I^-}{I^+ + I^-} = P\cos(\Delta\phi_a + \Delta\phi_g + \Delta\phi_s), \qquad (5)$$

where $\Delta\phi_g$ is the gravitation-induced phase shift, $\Delta\phi_a$ is a phase difference introduced by an additional magnetic field, and $\Delta\phi_s$ is a correction term due to the Sagnac effect introduced by the rotation of the Earth. The phase shift between

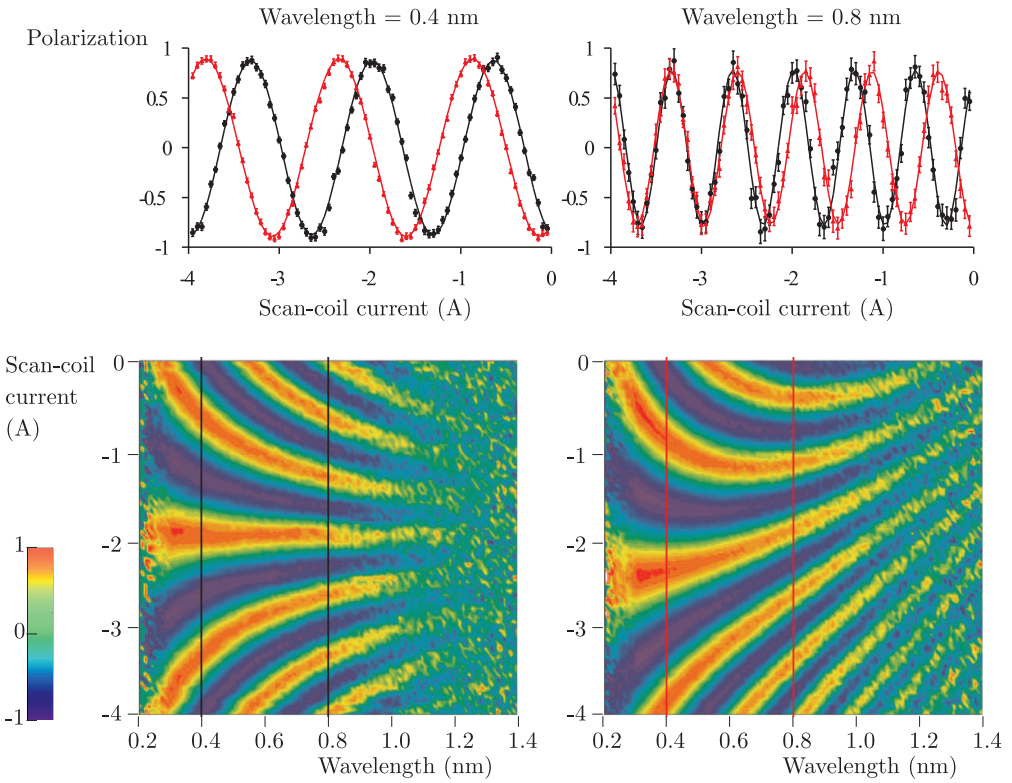

FIG. 3. (Color online) Measured polarization as a function of wavelength and scan-coil current for -0.5° inclination angle. For the bottom-left graph the beam was split in the horizontal direction, and for the bottom-right graph the beam was split in the vertical direction. The upper graphs show cuts along the black and red lines for wavelengths of 0.4 and 0.8 nm. The lines in the upper graphs are fits to the data points according to Eq. (7).

two neutron wave functions traversing different paths through an interferometer due to the Sagnac effect has been estimated as [4,20]

$$\Delta\phi_s = \frac{2mA\Omega}{\hbar}\{\sin\theta_L \sin h + \cos\theta_L \cos h \cos A_z\}, \qquad (6)$$

where $A = \delta L_{\text{split}}$ equals the area between the two trajectories, $\Omega = 72.92$ μrad/s equals the rotation frequency of the Earth, h the elevation of the normal to that area, and A_z the azimuth of that normal. For OffSpec $\theta_L = 51.57^{\circ}$, $A_z \approx 6^{\circ}$ (within $\pm 5^{\circ}$). h is 0° for the measurements in the vertical plane and 90° for the measurements in the horizontal plane. Hence the Sagnac effect introduces an additional spin-echo phase shift of $C_2\lambda^2$, where $C_2 = m\eta L_{\text{split}}\Omega(\cos\theta_L \sin h + \sin\theta_L \cos h \cos A_z)/\hbar$, yielding -0.0386 rad/nm^2 for the vertical case and 0.0489 rad/nm^2 for the horizontal one. It is a function of wavelength as the spin-echo length is a function of wavelength. The sign of the Sagnac phase shift with respect to the gravitational phase shift depends on the angle θ and the direction of the normal of area A with respect to the rotation direction of the Earth.

$\Delta\phi_a$ is used to increase the sensitivity by adding a phase difference introduced by means of an additional magnetic field B_a, created by a current I_a through a scan coil of effective length L_a. This scan coil was positioned in between the magnetic-field regions. The boundaries of this additional magnetic field were perpendicular to the beam direction so that no additional splitting is introduced. The additional phase difference due to this field is $\Delta\phi_a = B_a L_a \lambda m\mu/(2\pi\hbar^2)$.

The measured spin-echo phase difference as a function of wavelength is

$$\Delta\phi_a + \Delta\phi_g + \Delta\phi_s = (C_0 I_a + C_1)\lambda + C_2\lambda^2 + C_3\lambda^3, \qquad (7)$$

where $C_0 = \Delta\phi_a/(\lambda I_a) = (B_a/I_a)L_a mg\mu/(2\pi\hbar^2)$, C_1 represents the initial out-of-echo condition, and $C_3 = \Delta\phi_g/\lambda^3$ is determined by the gravitational phase shift only. Note that $C_3 = (1 - \alpha\tan\theta)(\eta L_{\text{Split}} m^2 g)/(2\pi\hbar^2)$ is a constant independent of neutron wavelength or scan-coil current. C_2 is due to the Sagnac effect introduced by the rotation of the Earth.

Measurements were performed for a series of scan-coil currents and several values of α. As an example, two series are shown in Fig. 3. The bottom-left graph shows the polarization as a function of wavelength and scan-coil current in case the beam was split in the horizontal direction; the bottom-right graph shows the same results with the same instrumental settings in case the beam was split in the vertical direction. The upper graphs show cuts along the black and red lines for wavelengths of 0.4 and 0.8 nm.

These results were fitted to Eq. (7) to obtain values for P, C_0, C_1, and C_3. Examples of such fits are shown in the top graphs of Fig. 3; they correspond with the cuts along the black and red lines for wavelengths of 0.4 and 0.8 nm in the bottom graphs.

For each instrument setting the measurement series was done with and without the grating in the beam. The initial out-of-echo condition C_1 only slightly changes between measurements. The differences occurring between the fit results with

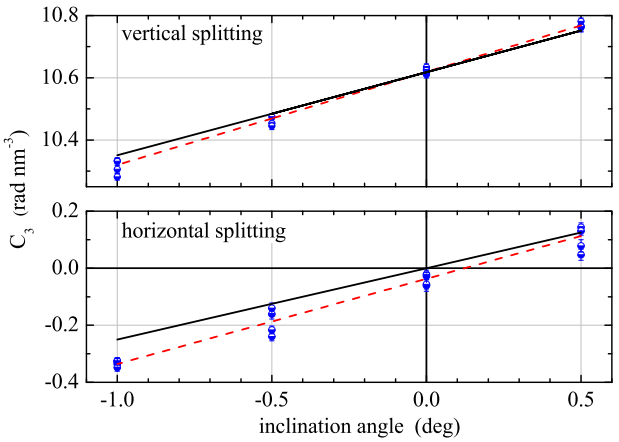

FIG. 4. (Color online) Fit results of C_3 (data points and error bars) as a function of inclination angle between the wave vector of the incident beam and the horizontal. The black full lines correspond to the theoretical values obtained with the calibrated value of the spin-echo-length constant and the local gravity constant. The red dashed lines are best fits.

and without grating in the beam are all within the experimental statistical deviations. The fitted P values with and without grating in the beam were used for the calibration of the spin-echo-length constant, as discussed in the previous section. C_0 was determined by separately fitting the data for each measurement series. The average result for the vertical splitting is 10.561(15) rad/(A nm), where the number between brackets is the standard deviation corresponding to 0.14%. As expected, C_0 did not depend on the inclination angle, so that for the fit of C_1 and C_3, C_0 was fixed for all vertical measurements to 10.561 rad/(A nm) to reduce statistical variation. The average result for the horizontal splitting is 11.612(33) rad/(A nm). Again, C_0 did not depend on the inclination angle, so that for the fit C_0 was fixed for all horizontal measurements to 11.612 rad/(A nm). The difference in C_0 between the vertical and horizontal series is due to the use of a (slightly) different scan-coil geometry.

The fit results for C_3 are shown in Fig. 4. The dots and error bars represent the fitted values and the black full lines represent the theoretical calculations using the calibrated spin-echo-length constants and the local gravity constant. The local gravity constant was determined by means of the Gravity Formula of 1980 [21], resulting in $g = 9.811\,9$ m/s^2 with an accuracy of about 0.002%. The inclination angle was measured with an accuracy of 0.1 mrad and the divergences of the neutron beam were limited to 2.8 mrad in the splitting direction and 0.8 mrad perpendicular to the splitting direction by means of two diaphragms of 5×12 mm^2 placed 6.39 m apart.

The dependence on the inclination angle is given by the slope of the lines. The slopes should be the same, as the coefficient of α does not depend on whether the splitting is in horizontal or vertical direction. This can be understood by taking into consideration that the effect occurs due to the increased velocity of the neutrons when they are falling down, resulting in a faster passage and hence a smaller number of precessions in the second magnetic-field region. If the dependence of the gravity phase shift on the inclination angle α as derived in the Appendix is not taken into account, the deviation with the measured value of C_3 reaches a maximum of –0.25 rad/nm^3 for an inclination angle of –1°. This corresponds to a deviation of 2.5% in the total effect.

V. DISCUSSION AND CONCLUSIONS

The red dashed lines in Fig. 4 are best fits. The slopes are taken equal and are 89% of the theoretical value. The calibration procedure is used to determine the spin-echo length that is needed to calculate the area A between the upper and lower trajectories of the neutron wave. This calibration is done to circumvent the fact that Eq. (4) is just approximately valid due to the way the instrument is actually constructed [22]. Because of the calibration, this equation is not needed to determine the spin-echo length. For the correction factor, however, the angle θ is needed, as the slope of the theoretical line is proportional to the tangent of that angle. Hence, this Eq. (4) is used to determine the effective angle θ for the correction. Hence, when the actual angle θ is a little less than the effective angle (52.2° instead of 55.3°), this has an effect on the slope but not on the intercept of the theoretical line. The value for 0 inclination angle for the vertical measurements is 10.619(9) rad/nm^3, which is in accordance with the theoretically expected one of 10.618(24) rad/nm^3. The uncertainty is mainly due to the uncertainty in the calibrated spin-echo length. Furthermore, the value for 0 inclination angle for the horizontal measurements is –0.037(15) rad/nm^3, while theoretically it should be 0 if the correction for the Sagnac effect is correct. If the correction of the Sagnac effect is omitted, the fitted value is –0.003 rad/nm^3, and when the correction is reversed it becomes +0.032 rad/nm^3. If the correction for the Sagnac effect is omitted in the results for the vertical splitting, the value of C_3 reduces to 10.592(9) rad/nm^3, also within range of the theoretically expected value. The difference between the theory and the intercept for the horizontal measurements is 2 standard deviations. Although the difference is small, it is remarkable that without the Sagnac corrections the theoretical values match measurements a little better. This could be due to several causes: the derivation of the Sagnac effect might be wrong (but the authors could not find an error in the derivation); or it is a statistical effect (this is a rather small but possible chance, about 5% due to the 2 standard deviation difference); or maybe the refraction of the neutron wave function at the magnetic-field boundary is influenced by the rotation of the Earth compensating the Sagnac effect, which is in contrast to the COW experiments where the Sagnac effect is due to refraction and reflection at nuclear potential steps.

Regardless of this uncertainty, the result for the gravitation-induced phase shift agrees within approximately 0.1% with the theoretically expected result, while the overall measurement accuracy is 0.25%. The fact that the statistical variation in C_3 is less than that for the calibration of the spin-echo length using a grating shows that this method can also be used to calibrate the spin-echo length with an accuracy of 0.1%. With the novel spin-echo neutron spectrometer OffSpec, it is possible to measure the gravitation-induced phase shift up to an accuracy of 0.1%. This accuracy is achieved by exploiting the high stability of the spin-echo spectrometer, in addition

to the use of the whole spectrum (roughly 0.2–1.0 nm) of the beam, not being limited to a monochromatic beam, as in a perfect-crystal interferometer experiment.

It was found that there is a significant dependence on the inclination angle with respect to the horizontal. For the experiment considered here, the deviation increases to a maximum of 2.5%. It has been shown in Appendix A that this effect also occurs for the COW experiment and should be taken into account for the data treatment of these measurements. A possible deviation could easily mount up to 0.5%, as the inclination angle for these measurements was not more accurately determined than 0.5° and the Bragg angle was about 30° [4]. This gives a possible explanation why COW experiments measure a too-small gravitation-induced phase shift.

This effect is not limited to neutron interferometry measurements but is valid for all interference experiments involving matter waves. To elucidate the effect for other particle interferometry experiments, the gravitational phase shift by inserting Eq. (4) can be expressed as

$$\Delta\phi_g = \frac{2L_{\text{split}}LB\cot\theta}{\hbar}\frac{\mu_n}{v^3}g(1-\alpha\tan\theta),$$

where v equals the velocity of the neutron. For constant instrument parameters, the phase shift scales with velocity to the third power, yielding larger phase shifts for slower particles. For instance, a cesium atom has approximately 133 times more mass than a neutron, reducing its velocity by more than a factor of 11.5 for the same kinetic energy, so that the expected phase shift for room-temperature cesium atoms is a factor of 1500 larger than for neutrons. Although the spin-echo method and beam splitting has been realized also for atom beams [23,24], the reported experiments were not designed to measure the gravitational phase shift. However, these kinds of experiments can be adapted to measure the effect.

ACKNOWLEDGMENTS

This research project has been supported by the European Commission under the 7th Framework Program through the Research Infrastructures action of the Capacities Program (Contract No. CP-CSA_INFRA-2008-1.1.1, No. 226507-NMI3). The authors would like to thank the United Kingdom Science and Technology Facilities Council (STFC) for the award of beam time, Dr. K. S. Knight for calibrating the aluminum sample on HRPD, and Prof. Dr. W. M. Snow, Indiana University, for bringing the possibility of this experiment to our attention.

APPENDIX: INFLUENCE OF BEAM INCLINATION ON GRAVITATION-INDUCED PHASE DIFFERENCE.

1. Optical phase acquired by a neutron following a path through a gravitation potential

In the semiclassical approximation, a neutron can be considered locally as a plane wave with a wave vector in the direction of propagation. The direction of the wave vector is the slope of the trajectory of the neutron. The length of the wave vector is determined by the local refractive index according to Eq. (2). Assume the trajectory is located in the (x,y) plane where the gravitation potential is given by $V_g = mgy$, with m the mass of the neutron and g the gravitation constant. The starting point of the trajectory is at (x_1,y_1) and the end point at (x_2,y_2). The optical phase acquired by a neutron following this trajectory is

$$\phi = \int_{(x_1,y_1)}^{(x_2,y_2)} \vec{k}\cdot d\vec{r},$$

where $\vec{r}$ describes the trajectory. As $d\vec{r}//\vec{k}, dr = \sqrt{dx^2+dy^2}$, and $k = k_x\sqrt{1+(dy/dx)^2}$, this can be rewritten as

$$\phi = k_x\int_{x_1}^{x_2}\left\{1+\left(\frac{dy}{dx}\right)^2\right\}dx.$$

If the trajectory is described by a straight line with slope $\tan\zeta$, this can be further reduced to

$$\phi = k_x\frac{x_2-x_1}{\cos^2\zeta} = k(x_1)\frac{x_2-x_1}{\cos\zeta}. \tag{A1}$$

Note that k_x is constant for the complete trajectory, as the gravitation acceleration acts only in the y direction.

2. Current experiment

To calculate the effect of beam inclination α with respect to the horizontal, it is assumed that the curvature of the path due to gravity can be neglected.

Performing the derivation presented here, taking into account the parabolic trajectories of the neutrons due to gravity instead of straight trajectories and the different kinetic and potential energies at the points of refraction to the magnetic-field boundaries is tedious but straightforward and results in exactly identical expressions up to first order in α and ϵ_z.

The path for each spin state is split into three regions represented below by suffix 1, 2, and 3, respectively.

The first region is the first magnetic-field region, where the path is inclined with respect to the horizontal with an angle $\alpha+\gamma_1^{\pm}$ (see also Fig. 1), where the refraction angle is given by Eq. (3)

$$\gamma_1^{\pm} = \pm\epsilon_z\cot\theta/2,$$

where n_0 was taken to be 1 and all terms of second or higher order in ϵ_z were neglected. The local refractive index at the splitting point (x_1,y_1) is determined by the height of the beam according to Eq. (2),

$$n^{\pm}(x_1,y_1) = 1\mp\epsilon_z/2 - Q_g y_1(1\pm\epsilon_z/2),$$

where $Q_g = m^2g/(\hbar^2k_0^2)$ and all terms of second or higher order in ϵ_z and $Q_g y_1$ were neglected. The wave vector just before splitting has been used as k_0. The phase acquired in this region, according to Eq. (A1), is (also using $\alpha \ll 1$)

$$\phi_1^{\pm} = k_0L[1\mp\epsilon_z/2 - Q_g y_1(1\pm\epsilon_z/2)],$$

where all second-order terms in ϵ_z, $Q_g y_1$, and α were neglected.

The second region is in between the magnetic-field regions, where the path is almost parallel to the beam before splitting—almost, as the refraction angle at this point is

$$\gamma_2^{\pm} = \mp\frac{\epsilon_z}{2n_2^2}\cot\theta,$$

where the difference is due to $n_2^2 = 1 - 2Q_g y(x_1 + L)$. Note that $\gamma_2^\pm$ has a reversed sign compared to $\gamma_1^\pm$ due to the fact that the neutrons are leaving the magnetic field. The path in region 2 can be described by $y(x) = y_1 + (\alpha + \gamma_1^\pm)(x - x_1) + \gamma_2^\pm(x - x_1 - L)$. According to Eq. (2),

$$n^\pm(x_1 + L) = 1 - Q_g y(x_1 + L).$$

The phase acquired in this region, according to Eq. (A1), is

$$\phi_2^\pm = k_0(L_{\text{split}} - L)[1 - (\alpha + \gamma_1^\pm)Q_g L - Q_g y_1].$$

The third region is in the second magnetic-field region, where the refraction angle is

$$\gamma_3^\pm = \mp\frac{\epsilon_z}{2n_3^2}\cot\theta,$$

where $n_3^2 = 1 - 2Q_g y(x_1 + L_{\text{split}})$. Note that $\gamma_3^\pm$ has the reversed sign compared to $\gamma_1^\pm$ because the magnetic field is reversed with respect to the first region. The path in region 3 can be described by $y(x) = y_1 + (\alpha + \gamma_1^\pm)(x - x_1) + \gamma_2^\pm(x - x_1 - L) + \gamma_3^\pm(x - x_1 - L_{\text{split}})$. According to Eq. (2),

$$n^\pm(x_1 + L_{\text{split}}) = 1 \pm \epsilon_z/2 - Q_g y(x_1 + L_{\text{split}})(1 \mp \epsilon_z/2),$$

also with the reversed sign for ϵ_z due to the reversed magnetic field. The phase acquired in this region is

$$\phi_3^\pm = k_0 L\{1 \pm \epsilon_z/2 - Q_g[y_1 + (\alpha + \gamma_1^\pm)L_{\text{split}} + \gamma_2^\pm(L_{\text{split}} - L)](1 \mp \epsilon_z/2)\}.$$

The sum over all three regions is

$$\phi^\pm = k_0\{(L + L_{\text{split}})(1 - Q_g y_1) - Q_g[(2L_{\text{split}} - L)\alpha \pm L_{\text{split}}\epsilon_z(\cot\theta - \alpha)]/2\},$$

so that the difference between spin-up and spin-down phases is

$$\Delta\phi = \phi^+ - \phi^- = -Q_g L_{\text{split}}\epsilon_z(\cot\theta - \alpha) = \frac{Am^2 g}{\hbar^2 k_0}(1 - \alpha\tan\theta),$$

where $A = L_{\text{split}}\delta$ equals the area between the path of the two spin states.

3. COW experiment

At a lattice with spacing d, first-order Bragg reflection can occur (see Fig. 5) if and only if

$$k\, d \sin\theta_B = \pi.$$

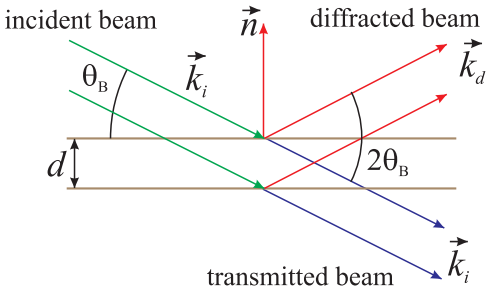

FIG. 5. (Color online) Bragg reflection at a lattice with spacing d.

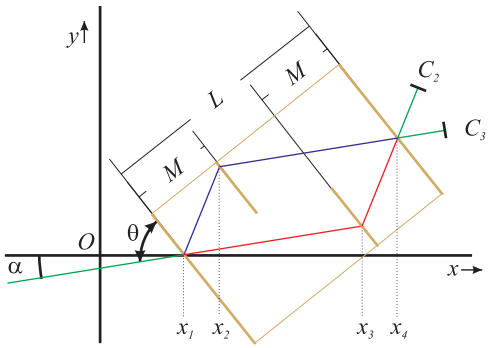

FIG. 6. (Color online) Trajectories of spin-wave components in the COW interferometer.

The wave vector of the transmitted beam is unaltered with respect to the incident beam. The angle between the wave vector of the reflected and transmitted beam is $2\theta_B$. The incident wave vector can be described by means of the slope, $\tan\zeta$, of the trajectory at the location of the intersection with the Bragg plane,

$$\vec{k}_i = k(\cos\zeta\ \vec{e}_x + \sin\zeta\ \vec{e}_y),$$

and hence the wave vector of the reflected beam is

$$\vec{k}_d = k\cos(2\theta_B + \zeta)\vec{e}_x + k\sin(2\theta_B + \zeta)\vec{e}_y,$$

so that the slope after Bragg reflection becomes

$$\tan\zeta' = \tan(2\theta_B + \zeta). \tag{A2}$$

The path of the neutron components through the COW interferometer is shown in Fig. 6. The neutron beam is split up at the first Bragg reflection, is reflected at the second Bragg reflection, and merges again at the third Bragg reflection. To calculate the phase difference between the two paths, it is assumed that the curvature of the trajectories can be neglected and that gravity does not influence the *effective* Bragg angle. The Bragg angle depends on the wave vector and hence on the local refractive index given by Eq. (2), and hence on the gravitation potential according to $\theta_B(y) = \theta_B(y_1) + Q_g(y - y_1)\tan\theta_B(y_1)$ up to first order in Q_g, where Q_g is defined in the previous section. However, for constructive interference behind the interferometer, it is required that both beams emerge parallel to each other and hence the *effective* Bragg angle at all positions should be the same (obtainable by the spread in direction of the Bragg planes) [25]. First, the optical phase of the upper or blue path is calculated, then that of the lower or red path, and finally the difference is taken to find the optical phase difference between the two paths.

a. Upper or blue path

The incident angle on the Bragg planes is determined by the slope $\tan\alpha$ of the trajectory at $x = x_1$. To determine the starting slope of the first upper or blue trajectory, the reflected angle can be calculated by Eq. (A2). The equation of the first upper or blue trajectory is

$$y = y_1 + (x - x_1)\tan(2\theta_B + \alpha).$$

The location of the next boundary is given by

$$y = y_1 + (x_1 - x)\tan(\theta - \alpha) + \frac{M}{\cos(\theta - \alpha)}.$$

Note that for Bragg reflection to occur, $\theta = \pi/2 - \theta_B$. The trajectory of the neutron intersects this boundary at (x_2, y_2), for which the following holds:

$$x_2 = x_1 + M\frac{\cos(2\theta_B + \alpha)}{\cos\theta_B}, \quad y_2 = y_1 + M\frac{\sin(2\theta_B + \alpha)}{\cos\theta_B}.$$

The phase acquired on this trajectory, according to Eq. (A1), is

$$\phi_{12} = k_0 M\frac{1 - Q_g y_1}{\cos\theta_B}.$$

After this, the neutron is Bragg reflected into the second upper or blue trajectory starting at $x = x_2$. The slope of this trajectory can be calculated using Eq. (A2), replacing θ_B by $-\theta_B$, as the normal to the Bragg planes is now in the opposite direction. The equation is

$$y = y_2 + (x - x_2)\tan\alpha.$$

The location for the next boundary for the intersection at (x_4, y_4) is given by

$$y = y_1 + (x_1 - x)\tan(\theta - \alpha) + \frac{L}{\cos(\theta - \alpha)},$$

so that

$$x_4 = x_2 + (L - M)\frac{\cos\alpha}{\cos\theta_B}, \quad y_4 = y_2 + (L - M)\frac{\sin\alpha}{\cos\theta_B}.$$

The phase acquired on this trajectory is

$$\Phi_{24} = k_0(L - M)\frac{1 - Q_g y_2}{\cos\theta_B}.$$

b. Lower or red path

The equation of the first lower or red trajectory is

$$y = y_1 + (x - x_1)\tan\alpha.$$

The location for the next boundary for the intersection at (x_3, y_3) is given by

$$y = y_1 + (x_1 - x)\tan(\theta - \alpha) + \frac{L - M}{\cos(\theta - \alpha)},$$

so that

$$x_3 = x_1 + (L - M)\frac{\cos\alpha}{\cos\theta_B}, \quad y_3 = y_1 + (L - M)\frac{\sin\alpha}{\cos\theta_B}.$$

The phase acquired on this trajectory is

$$\Phi_{13} = k_0(L - M)\frac{1 - Q_g y_1}{\cos\theta_B}.$$

After this, the neutron is Bragg reflected into the second upper or red trajectory starting at (x_3, y_3). The slope of this trajectory can be calculated by using Eq. (A2). This equation is

$$y = y_3 + (x - x_3)\tan(2\theta_B + \alpha). \tag{A3}$$

The location for the next boundary for the intersection at (x_4, y_4) has been given before, and this intersection occurs at exactly the same location as of the other beam so that interference is obtained. The phase acquired on this trajectory is

$$\Phi_{34} = k_0 M\frac{1 - Q_g y_3}{\cos\theta_B},$$

so that the phase difference between the two trajectories is

$$\begin{aligned}\Delta\Phi &= \Phi_{13} + \Phi_{34} - \Phi_{12} - \Phi_{24} \\ &= \frac{Am^2 g}{\hbar^2 k_0}\cos\alpha(1 - \tan\theta_B\tan\alpha),\end{aligned}$$

where $A = 2M(L - M)\tan\theta_B$ equals the area between the two trajectories.

[1] J. Dabbs, J. Harvey, D. Paya, and H. Horstmann, Phys. Rev. **139**, B756 (1965).

[2] L. Koester, Phys. Rev. D **14**, 907 (1976).

[3] J. Schiedmayer, Nucl. Instrum. Methods Phys. Res., Sect. A **284**, 59 (1989).

[4] R. Colella, A. Overhauser, and S. Werner, Phys. Rev. Lett. **34**, 1472 (1975).

[5] G. van der Zouw, M. Weber, J. Felber, R. Gahler, P. Geltenbort, and A. Zeilinger, Nucl. Instrum. Methods Phys. Res., Sect. A **440**, 568 (2000).

[6] K. C. Littrell, B. E. Allman, O. I. Motrunich, and S. A. Werner, Acta Crystallogr., Sect. A **54**, 563 (1998).

[7] J. Springer, M. Zawisky, R. Farthofer, H. Lemmel, M. Suda, and U. Kuetgens, Nucl. Instrum. Methods Phys. Res., Sect. A **615**, 307 (2010).

[8] W. Schleich, D. Greenberger, and E. Rasel, New J. Phys. **15**, 013007 (2013).

[9] V. A. Kostelecky and J. D. Tasson, Phys. Rev. D **83**, 016013 (2011).

[10] R. Dalgliesh, S. Langridge, J. Plomp, V. de Haan, and A. van Well, Phys. B: Condens. Matter **406**, 2346 (2011).

[11] R. M. Dalgliesh and S. Langridge, OffSpec: Spin-echo Reflectometer at ISIS Second Target Station, 2014, http://www.isis.stfc.ac.uk/instruments/offspec/offspec3048.html.

[12] R. Gahler, R. Golub, K. Habicht, T. Keller, and J. Felber, Physica B **229**, 1 (1996).

[13] V. F. Sears, *Neutron Optics*, 1st ed. (Oxford University Press, Oxford, UK, 1989).

[14] J. L. Staudenmann, S. A. Werner, R. Colella, and A. W. Overhauser, Phys. Rev. A **21**, 1419 (1980).

[15] J. R. Santisteban, L. Edwards, A. Steuwer, and P. J. Withers, J. Appl. Crystallogr. **34**, 289 (2001).

[16] M. W. Johnson and W. I. F. David, "HRPD: The high resolution powder diffractometer at the SNS", Rutherford Appleton Laboratory, Report 1985, RAL-85-112.

[17] M. T. Rekveldt, Nucl. Instrum. Methods Phys. Res., Sect. B **114**, 366 (1996).
[18] V. O. de Haan, J. Plomp, W. G. Bouwman, M. Trinker, M. T. Rekveldt, C. P. Duif, E. Jericha, H. Rauch, and A. A. van Well, J. Appl. Crystallogr. **40**, 151 (2007).
[19] V. O. de Haan, A. A. van Well, and J. Plomp, Phys. Rev. B **77**, 104121 (2008).
[20] S. Werner, Gen. Relativ. Gravit. **40**, 921 (2008).
[21] H. Moritz, J. Geodesy. **74**, 128 (2000).
[22] J. Plomp, V. de Haan, R. Dalgliesh, S. Langridge, and A. van Well, Phys. B: Condens. Matter **406**, 2354 (2011).
[23] A. D. Cronin, J. Schmiedmayer, and D. E. Pritchard, Rev. Mod. Phys. **81**, 1051 (2009).
[24] D. Kokorowski, T. Roberts, R. Rubenstein, E. Smith, and E. Pritchard, Fortschr. Phys. **48**, 615 (2000).
[25] D. Greenberger and A. Overhauser, Rev. Mod. Phys. **51**, 43 (1979).